Phase separation and nanocrystallization in Al92Sm8 metallic glass

Jerzy Antonowicz, a R Yavari, Walter Botta, Pierre Panine

Phase separation and nanocrystallization in $Al_{92}Sm_8$ metallic glass

Journal:	*Philosophical Magazine & Philosophical Magazine Letters*
Manuscript ID:	TPHM-05-Jun-0296.R1
Journal Selection:	Philosophical Magazine
Date Submitted by the Author:	09-Sep-2005
Complete List of Authors:	Antonowicz, Jerzy; Warsaw University of Technology, Faculty of Physics Yavari, A R; INPG, LTPCM Botta, Walter; INPG, LTPCM; Universidade Federal de Sao Carlos, DEMa Panine, Pierre; ESRF
Keywords:	X-ray scattering, nanocrystallization, metallic glasses, phase decomposition
Keywords (user supplied):	Small-angle X-ray scattering

Phase separation and nanocrystallization in $Al_{92}Sm_8$ metallic glass

Jerzy Antonowicz

Faculty of Physics, Warsaw University of Technology, Koszykowa 75, 00-662 Warsaw, Poland

Alain Reza Yavari, **Walter José Botta***

Institut National Polytechnique de Grenoble, (LTPCM-CNRS umr 5614), 1130 Rue de la Piscine, BP 75, 38402 St-Martin-d'Hères Campus, France

Pierre Panine

European Synchrotron Radiation Facility, 38042 Grenoble, France

*Permanent address: Universidade Federal de Saõ Carlos, DEMa, CP 676, 13.565-905 Saõ Carlos, SP, Brazil.

Abstract

Crystallization of $Al_{92}Sm_8$ metallic glass was investigated *in-situ* using combined small-angle and wide-angle X-ray scattering (SAXS/WAXS) techniques during isothermal annealing at temperatures close to crystallization point. A continuously growing interference maximum shifting progressively toward lower angles was found to develop in SAXS regime. Simultaneously taken WAXS spectra reveal formation of fcc-Al nanocrystalline phase. The analysis of the SAXS/WAXS data indicate that amorphous phase separation is responsible for the nanocrystalline microstructure formation. The primary fcc-Al crystals nucleate inside the Al-rich amorphous regions formed during alloy decomposition and their growth is constrained by the region size.

1 Introduction

Evidences of amorphous phase separation in numerous metallic glasses based on small-angle X-ray and neutron scattering [1, 2, 3], X-ray diffraction [3], differential scanning calorimetry [4], transmission electron microscopy [5] and atom probe field ion microscopy [6] were reported over previous years. Some of these results were recently questioned by 3D-atom probe study [7]. An influence of the amorphous phase decomposition on the crystallization behaviour was also discussed [2, 3, 8, 9]. The studies suggest a relation between the scale of glassy phase separation and the crystallites size.

Aluminum-based metallic glasses containing rare earth or rare earth and transition metals additions are known to exhibit interesting mechanical properties [10]. These properties can be further tailored by thermal annealing to generate ultra-fine ($\sim$ 10 nm) fcc-Al nanocrystals of a density of about $10^{22} - 10^{23}$ m^{-3} embedded in an amorphous matrix. This kind of microstructure requires high nucleation frequency and low growth rate. Nanocrystallization of the Al-based glasses was previously attributed to heterogeneous nucleation [11], quenched-in nuclei [12] and a new type of homogeneous nucleation [13]. Phase separation in Al-Gd-La-Ni glass was reported with nanocrystal nucleating preferentially on the boundaries between the two phases [14, 15].

However the results from 3D-atom probe for similar alloy system did not provide an evidence of the amorphous phase separation [16]. The rapid nanocrystal growth arrest was explained by overlapping of the diffusion fields of the adjecent crystals [17]. In this paper we briefly report results from *in-situ* small-angle and wide-angle X-ray scattering (SAXS/WAXS) measurements supported by transmission electron microscopy (TEM) analysis.

2 Experimental

An ingot of $Al_{92}Sm_8$ alloy was prepared from pure elements using an arc melting device. Amorphous samples in form of about 25 μm thick ribbons were obtained by rapid quenching using the "melt-spinning" method. The liquid alloy was ejected by argon pressure on the surface of a massive copper wheel spinning at of 33 m/s. The SAXS/WAXS experiment was carried out in transmission at the ID02 beamline of the European Synchrotron Radiation Facility using wavelength of $\lambda = 1.00$Å. The small pieces of as-quenched ribbons were sealed in glassy capillaries under argon atmosphere. Samples were placed in a hot-stage holder between the incident beam and SAXS/WAXS detectors. The annealing temperature was reached with 100 K/min heating

rate. The q-range covered $0.07 - 2.1$ nm^{-1} ($q = (4\pi/\lambda)\sin\theta$ and θ is half the scattering angle) in case of SAXS while WAXS measurements covered $5 - 54$ deg of 2θ range. The TEM specimen prepared by ion-milling was analysed in a Jeol 3010 microscope.

3 Results and Discussion

Figure 1 shows the time evolution of SAXS spectra during isothermal annealing at 443 K of an as-quenched sample after subtraction of weak glassy capillary signal. At the moment of reaching the annealing temperature the SAXS pattern does not show any diffrence from the as-quenched one and indicates a uniform composition of the sample. 40 s after reaching the annealing temperature the SAXS intensity $I(q)$ exhibits a growing interference maximum centered at $q = 0.62$ nm^{-1}. After 100 s the peak continues to develop growing with time and shifting toward the origin in q space. The presence of a significant constant signal contribution at low q is attributed to scattering from the sample surface imperfections. Simultaneously to the appearance of the small-angle intensity maximum, fcc-Al Bragg peaks were found to develop on the initially amorphous pattern in the wide-angle regime (Figure

2). The traces of the Bragg peaks appearing for the as-quenched sample are probably due to single Al crystals formed during melt-spinning process on the amorphous ribbon edge, nevertheless this effect is negligible. Basing on the crystalline volume fraction calculation method [19] we estimated the lowest detectable crystalline content as 0.5%. Similar SAXS/WAXS spectra evolution was observed for other annealing temperatures (453 K and 463 K).

In order to determine the scattering objects' size the SAXS data were analysed using the Guinier approximation [20] where $I(q) \propto \exp(R_g^2 q^2/3)$ with R_g standing for a radius of gyration. For the spherical objects of radius R $R_g = \sqrt{3/5}R$. Figure 4 presents the compositional fluctuation size evaluated using the Guinier method together with mean crystal size calculated from (200) fcc-Al Bragg peak broadening using standard Scherrer formula. As shown in the figure the size values obtained from Guinier approximation are always higher than those resulting from the Scherrer method. A TEM image of sample annealed at 460 K for 1200 s together with corresponding selected area diffraction pattern is shown in Figure 3. The nanocrystal size determined from TEM is equal to 11.5 ± 1.5 nm which confirms the validity of the WAXS peak broadening method.

The observed SAXS spectra evolution is reminiscent for phase separation

occurring by spinodal mechanism. The existence of a constant compositional wavelength of $L = 2\pi/0.62\text{nm}^{-1} \approx 10$ nm with spontaneously growing amplitude as found in the early stage of transformation at 443 K is consistent with Cahn's linear theory of spinodal decomposition [21]. During the late stages of the decomposition the coarsening of the decomposed regions occurs which is manifested by the SAXS peak position decay. Many studies show that the magnitude of the q-vector q_m correspondidg to the maximum of the SAXS signal during the late stages of decomposition evolves with time as [18]: $q_m \propto t^{-a}$. In order to determine the value of a exponent, $\log q_m$ versus $\log t$ was plotted (inset in Figure 4). The plot corresponding to 443 K exhibits wide range of linearity with the slope $a = 0.21$ which is close to exponent values reported in systems undergoing spinodal decomposition [18]. Values ranging from 1/6 to 1/3 were observed for crystalline metallic systems, while $a \approx 0.23$ was reported in a borate glass [18]. The slope of the plot for 463 K decreases rapidly finally reaching zero which is attributed to advanced crystallization blocking the decomposed regions coarsening.

The Cahn's linear theory of spinodal decomposition predicts an exponential growth of the SAXS intensity: $I(q) \propto |c - c_0|^2 \propto \exp(2R(q)t)$, where $c - c_0$ is the deviation from the homogeneous concentration c_0, $R(q)$ is the

q-dependent concentration fluctuation growth rate and t is time. The growth rate $R(q)$ is related to D – the modulus of the (negative) chemical interdiffusion coefficient ($D = |\tilde{D}|$) by: $R(q)/q^2 = D[1 - q^2/(2q_m^2)]$. Thus, by plotting $R(q)/q^2$ vs q^2 ("Cahn plot") one can obtain D from the straight line fit. While according to the linear theory of spinodal decomposition the "Cahn plot" should be a straight line, its' typically observed shape is not linear [18]. It was shown that the experimental data may be successfully analysed by looking at the tangents at the peak position q_m [22].

We have found that at T=443 K the SAXS intensity grows exponentially with time during inital 600 s. At higher temperatures the exponential fit was possible only for shorter times. Figure 5 shows the increase of the SAXS intensity at T=443 K for different values of q and the resulting "Cahn plot" is presented in Figure 6. Both from the tangent y axis itercept and the slope $D = 4 \cdot 10^{-21}$ [m^{2}s^{-1}] was obtained. The validity of this estimation can be checked by comparing the mean diffusion distance $\bar{x} = \sqrt{6Dt}$ with the characteristc dimension of the decomposed system. Using the evaluated value of D and t=7200 s, one gets $\bar{x} \approx 13$ nm which is in excellent agreement with the results from the Guinier method (see Figure 4).

Our previous results from X-ray diffraction and TEM [23] revealed that

$Al_{92}Sm_8$ glass devitrification kinetics is controlled by fcc-Al nanocrystal nucleation rate. The glass crystallization proceeds by gradual increase of crystallite density and decreasing average distance between crystals. At first, such a crystallization model appears to be inconsistent with present SAXS results. This apparent discrepancy can be resolved if one considers a coupling of amorphous phase separation and progressive crystallization of one of the decomposed phases. It can be reasoned that the SAXS interference maximum is partially due to spatially correlated amorphous regions and partially to nanocrystals nucleating preferentially inside the Al-rich zones. The local increase in the nucleation rate can be due to high Al diffusivity or/and reduced crystal-glass interfacial energy. The growth of the crystallites is constrained by the zone size because of the samarium atoms with sluggish atomic diffusion outside Al-rich regions. The decomposed structure coarsening proceeds parallel to crystallization which progressively further slows down glass decomposition. Our present results may reinforce some of the conclusions from electrical resistivity measurements [24] where considering of the amorphous phase decomposition gives better agreement with experimental data.

4 Conclusions

In conclusion, we suggest that amorphous phase separation is a mechanism triggering and controlling nanocrystallization of $Al_{92}Sm_8$ metallic glass. The model proposed here explains both high nucleation rate and rapid arrest of growth required for nanocrystalline microstructure formation.

5 Acknowledgments

J. Antonowicz gratefully acknowledges the Polish Committee of Scientific Research (grant no: 7T08 A02121) and Faculty of Physics of Warsaw University of Technology.

References

[1] C.-P.P. Chou, D. Turnbull, *J. Non-Cryst. Solids* **17** 169 (1975)

[2] S. Schneider, P. Thiyagarajan, W.L. Johnson, *Appl. Phys. Lett.* **68** 493 (1996)

[3] A.R. Yavari, *Acta. Metall.* **36** 1863 (1988)

[4] H.S. Chen, *Mater. Sci. Eng.* **23** 151 (1976)

[5] L. Tanner, R. Ray, *Scripta. Met.* **14** 657 (1980)

[6] R. Bush, S. Schneider, A. Peker, W.L. Johnson, *Appl. Phys. Lett.* **63** 1544 (1995)

[7] I. Martin, T. Ohkubo, M. Ohnuma, B. Deconihout, K. Hono, *Acta Mater.* **52** 4427 (2004)

[8] J. Löffler, W.L. Johnson, *Appl. Phys. Lett.* **76** 3394 (2000)

[9] U. Köster, *Mater. Sci. Forum* **235-238** 377 (1997)

[10] A. Inoue, *Progr. Mater. Sci.* **43** 365 (1998)

[11] M. Calin, U. Köster, *Mater. Sci. For.* **269-272** 749 (1998)

[12] G. Wilde, R.I. Wu, J.H. Perepezko, Proceedings of 22nd Risø International Symposium on Materials Science: Science of Metastable and Nanocrystalline Alloys Structure, Properties and Modelling, Editors: A.R. Dinesen, M. Eldrup, D. Juul Jensen, S. Linderoth, T.B. Pedersen, N.H. Pryds, A. Schrøoder Pedersen and J.A. Wert, Risø National Laboratory, Roskilde, Denmark 2001

[13] K.F. Kelton, *Phil. Mag. Lett.* **77** 337 (1998)

[14] T.K. Croat, A.K. Gangopadhyay, K.F. Kelton, *Phil. Mag. A* **82** 2483 (2002)

[15] K.F. Kelton, T.K. Croat, A.K. Gangopadhyay, L.-Q. Xing, A.L. Greer, M. Weyland, X. Li, K. Rajan, *J. Non-Cryst. Solids* **317** 71 (2003)

[16] T. Gloriant, D.H. Ping, K. Hono, A.L. Greer, M.D. Baró, *Mater. Sci. Eng.* **A304-306** 315 (2001)

[17] D.R. Allen, J.C. Foley, J.H. Perepezko, *Acta Mater.* **46** 431 (1998)

[18] K. Binder, P. Fratzl, *Spinodal Decomposition* in *Phase Transformations in Materials*, edited by G. Kostorz, pp. 409-480, Wiley-VCH, Weinheim, (2001).

[19] J. Antonowicz, *J. Non-Cryst. Solids* **351** 2383 (2005)

[20] A. Guinier and G. Fournet, *Small-Angle Scattering of X-Rays*, John Wiley & Sons, New York (1995)

[21] J.W. Cahn, *Acta Metall.* **9** 795 (1961)

[22] J.S. Langer, M. Bar-on, H.D. Miller, *Phys. Rev. A* **11** 1417 (1975)

[23] J. Antonowicz, A.R. Yavari, G. Vaughan, *Nanotechnology* **15** 1038 (2004)

[24] L. Łukaszuk, K. Pękała, *Nanotechnology* **16** 169 (2005)

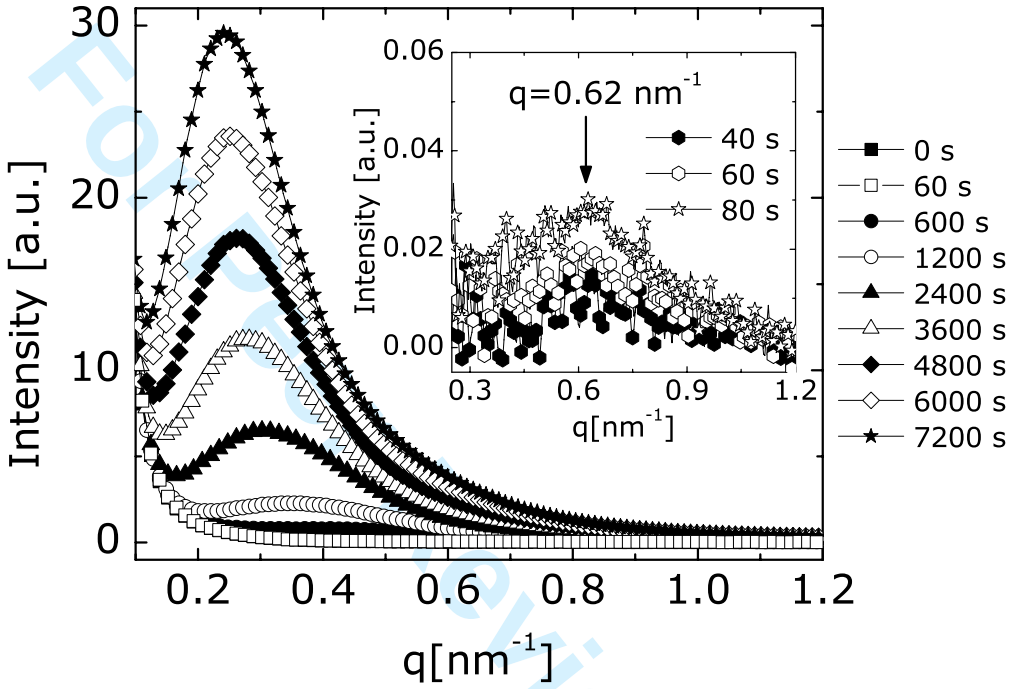

Figure 1: SAXS spectra evolution during isothermal annealing at 443 K of an as-quenched $Al_{92}Sm_8$. The inset presents early stages of SAXS maximum development when the peak is centered at $q = 0.62$ nm^{-1}.

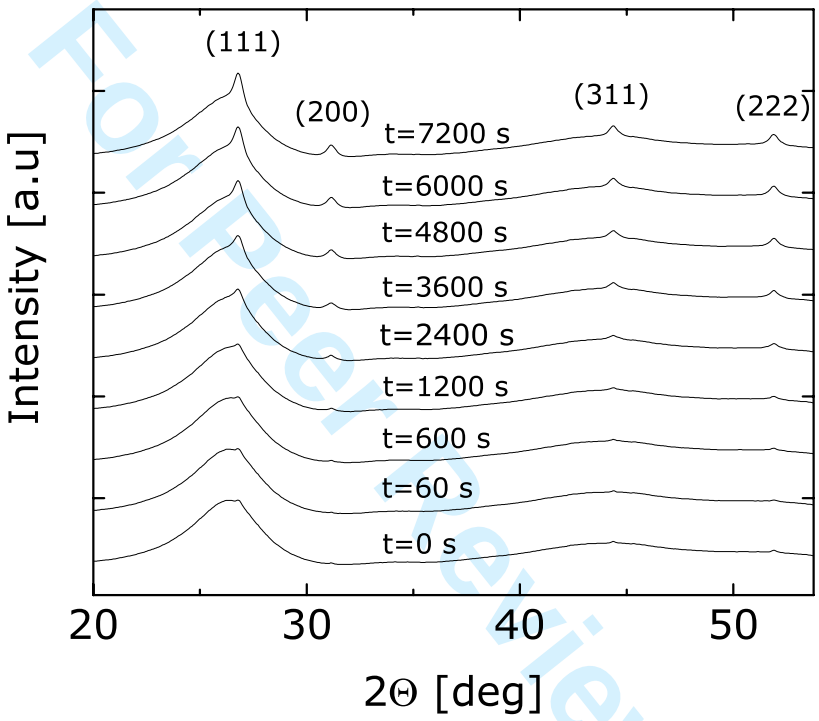

Figure 2: WAXS intensity data obtained during isothermal annealing at 443 K of an as-quenched $Al_{92}Sm_8$. The fcc-Al Bragg peaks are indexed.

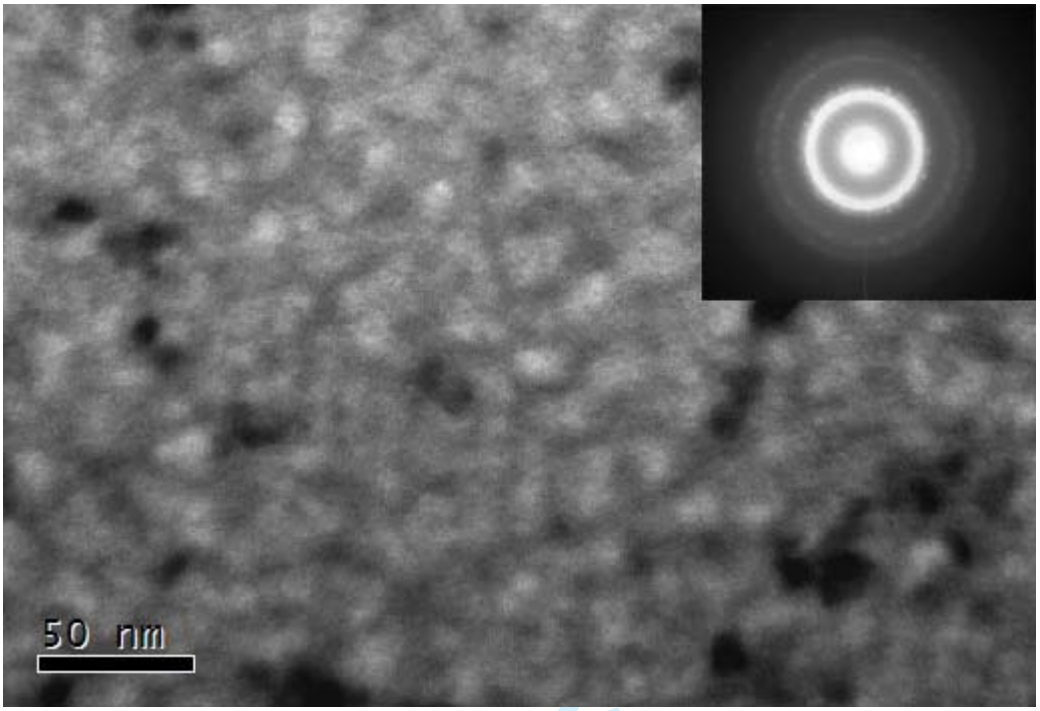

Figure 3: Bright field TEM image of $Al_{92}Sm_8$ glassy sample annealed at 460 K for 1200 s. The nanocrystal size determined from the micrograph is equal 11.5 ± 1.5 nm. The inset shows corresponding selected area diffraction pattern.

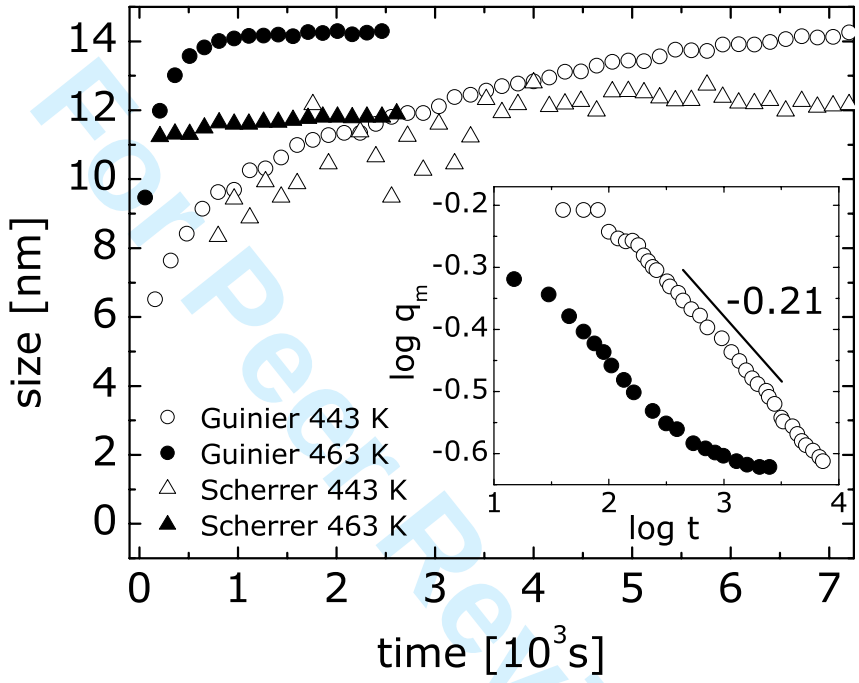

Figure 4: The compositional fluctuation size evolution obtained from the Guinier approximation (circles) and crystal size from the Scherrer method (triangles). The inset shows $\log q_m$ vs $\log t$ plot with the slope value indicated. Open symbols: annealing at 443 K, full symbols: annealing at 463 K.

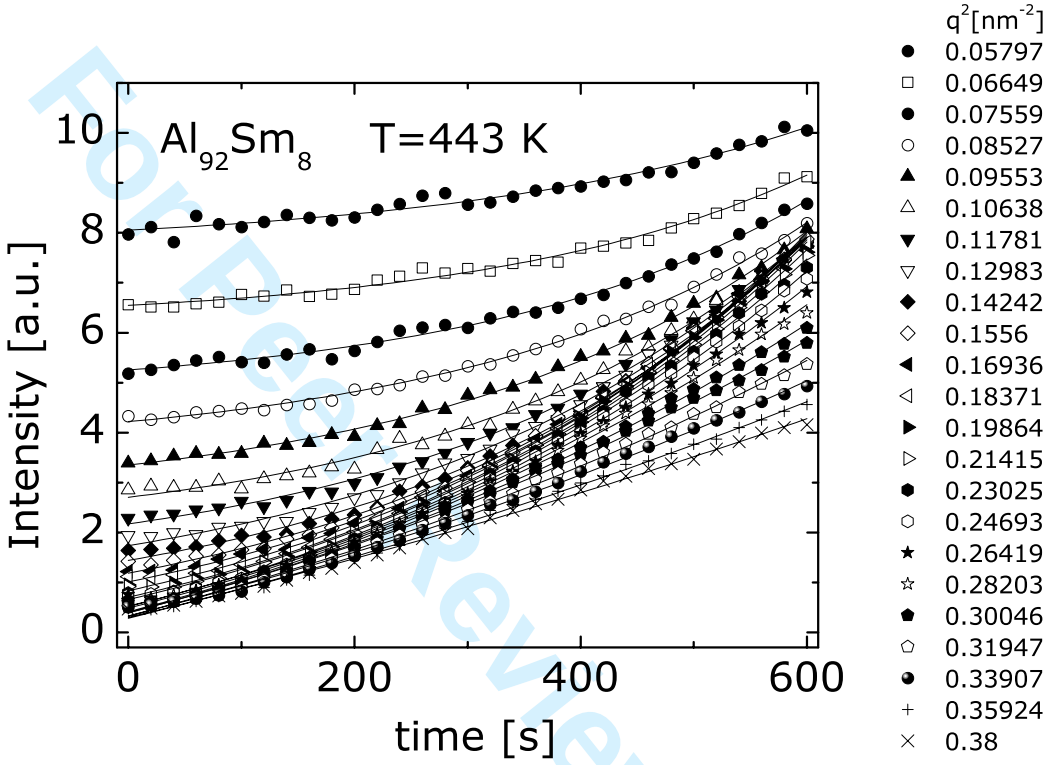

Figure 5: The increase of the SAXS intensity at T=443 K for different values of q (symbols). The lines are exponential fits.

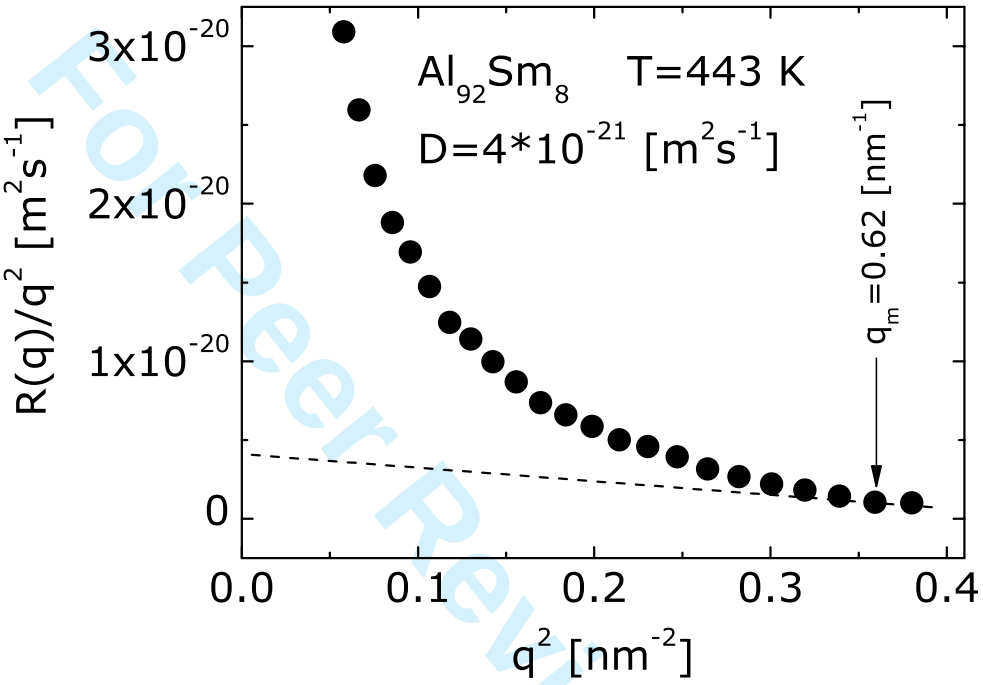

Figure 6: The "Cahn plot" obtained for T=443 K. The dashed line is a tangent to the curve at $q_m = 0.62$ nm $^{-1}$. The resulting diffusion coefficient is $D = 4 \cdot 10^{-21}$ [m^{2}s^{-1}]

List of Figures

6 The "Cahn plot" obtained for T=443 K. The dashed line is a tangent to the curve at $q_m = 0.62$ nm $^{-1}$. The resulting diffusion coefficient is $D = 4 \cdot 10^{-21}$ [m^{2}s^{-1}] 19

Phase separation and nanocrystallization in $Al_{92}Sm_8$ metallic glass

Jerzy Antonowicz

Faculty of Physics, Warsaw University of Technology, Koszykowa 75, 00-662 Warsaw, Poland

Alain Reza Yavari, **Walter José Botta***

Institut National Polytechnique de Grenoble, (LTPCM-CNRS umr 5614), 1130 Rue de la Piscine, BP 75, 38402 St-Martin-d'Hères Campus, France

Pierre Panine

European Synchrotron Radiation Facility, 38042 Grenoble, France

*Permanent address: Universidade Federal de Saõ Carlos, DEMa, CP 676, 13.565-905 Saõ Carlos, SP, Brazil.

Abstract

Crystallization of $Al_{92}Sm_8$ metallic glass was investigated *in-situ* using combined small-angle and wide-angle X-ray scattering (SAXS/WAXS) techniques during isothermal annealing at temperatures close to crystallization point. A continuously growing interference maximum shifting progressively toward lower angles was found to develop in SAXS regime. Simultaneously taken WAXS spectra reveal formation of fcc-Al nanocrystalline phase. The analysis of the SAXS/WAXS data indicate that amorphous phase separation is responsible for the nanocrystalline microstructure formation. The primary fcc-Al crystals nucleate inside the Al-rich amorphous regions formed during alloy decomposition and their growth is constrained by the region size.

1 Introduction

Evidences of amorphous phase separation in numerous metallic glasses based on small-angle X-ray and neutron scattering [1, 2, 3], X-ray diffraction [3], differential scanning calorimetry [4], transmission electron microscopy [5] and atom probe field ion microscopy [6] were reported over previous years. Some of these results were recently questioned by 3D-atom probe study [7]. An influence of the amorphous phase decomposition on the crystallization behaviour was also discussed [2, 3, 8, 9]. The studies suggest a relation between the scale of glassy phase separation and the crystallites size.

Aluminum-based metallic glasses containing rare earth or rare earth and transition metals additions are known to exhibit interesting mechanical properties [10]. These properties can be further tailored by thermal annealing to generate ultra-fine ($\sim$ 10 nm) fcc-Al nanocrystals of a density of about $10^{22} - 10^{23}$ m^{-3} embedded in an amorphous matrix. This kind of microstructure requires high nucleation frequency and low growth rate. Nanocrystallization of the Al-based glasses was previously attributed to heterogeneous nucleation [11], quenched-in nuclei [12] and a new type of homogeneous nucleation [13]. Phase separation in Al-Gd-La-Ni glass was reported with nanocrystal nucleating preferentially on the boundaries between the two phases [14, 15].

However the results from 3D-atom probe for similar alloy system did not provide an evidence of the amorphous phase separation [16]. The rapid nanocrystal growth arrest was explained by overlapping of the diffusion fields of the adjecent crystals [17]. In this paper we briefly report results from *in-situ* small-angle and wide-angle X-ray scattering (SAXS/WAXS) measurements supported by transmission electron microscopy (TEM) analysis.

2 Experimental

An ingot of $Al_{92}Sm_8$ alloy was prepared from pure elements using an arc melting device. Amorphous samples in form of about 25 μm thick ribbons were obtained by rapid quenching using the "melt-spinning" method. The liquid alloy was ejected by argon pressure on the surface of a massive copper wheel spinning at of 33 m/s. The SAXS/WAXS experiment was carried out in transmission at the ID02 beamline of the European Synchrotron Radiation Facility using wavelength of $\lambda = 1.00$Å. The small pieces of as-quenched ribbons were sealed in glassy capillaries under argon atmosphere. Samples were placed in a hot-stage holder between the incident beam and SAXS/WAXS detectors. The annealing temperature was reached with 100 K/min heating

rate. The q-range covered $0.07 - 2.1$ nm^{-1} ($q = (4\pi/\lambda)\sin\theta$ and θ is half the scattering angle) in case of SAXS while WAXS measurements covered $5 - 54$ deg of 2θ range. The TEM specimen prepared by ion-milling was analysed in a Jeol 3010 microscope.

3 Results and Discussion

Figure 1 shows the time evolution of SAXS spectra during isothermal annealing at 443 K of an as-quenched sample after subtraction of weak glassy capillary signal. At the moment of reaching the annealing temperature the SAXS pattern does not show any diffrence from the as-quenched one and indicates a uniform composition of the sample. 40 s after reaching the annealing temperature the SAXS intensity $I(q)$ exhibits a growing interference maximum centered at $q = 0.62$ nm^{-1}. After 100 s the peak continues to develop growing with time and shifting toward the origin in q space. The presence of a significant constant signal contribution at low q is attributed to scattering from the sample surface imperfections. Simultaneously to the appearance of the small-angle intensity maximum, fcc-Al Bragg peaks were found to develop on the initially amorphous pattern in the wide-angle regime (Figure

2). The traces of the Bragg peaks appearing for the as-quenched sample are probably due to single Al crystals formed during melt-spinning process on the amorphous ribbon edge, nevertheless this effect is negligible. Basing on the crystalline volume fraction calculation method [19] we estimated the lowest detectable crystalline content as 0.5%. Similar SAXS/WAXS spectra evolution was observed for other annealing temperatures (453 K and 463 K).

In order to determine the scattering objects' size the SAXS data were analysed using the Guinier approximation [20] where $I(q) \propto \exp(R_g^2 q^2/3)$ with R_g standing for a radius of gyration. For the spherical objects of radius R $R_g = \sqrt{3/5}R$. Figure 4 presents the compositional fluctuation size evaluated using the Guinier method together with mean crystal size calculated from (200) fcc-Al Bragg peak broadening using standard Scherrer formula. As shown in the figure the size values obtained from Guinier approximation are always higher than those resulting from the Scherrer method. A TEM image of sample annealed at 460 K for 1200 s together with corresponding selected area diffraction pattern is shown in Figure 3. The nanocrystal size determined from TEM is equal to 11.5 ± 1.5 nm which confirms the validity of the WAXS peak broadening method.

The observed SAXS spectra evolution is reminiscent for phase separation

occurring by spinodal mechanism. The existence of a constant compositional wavelength of $L = 2\pi/0.62\text{nm}^{-1} \approx 10$ nm with spontaneously growing amplitude as found in the early stage of transformation at 443 K is consistent with Cahn's linear theory of spinodal decomposition [21]. During the late stages of the decomposition the coarsening of the decomposed regions occurs which is manifested by the SAXS peak position decay. Many studies show that the magnitude of the q-vector q_m correspondidg to the maximum of the SAXS signal during the late stages of decomposition evolves with time as [18]: $q_m \propto t^{-a}$. In order to determine the value of a exponent, $\log q_m$ versus $\log t$ was plotted (inset in Figure 4). The plot corresponding to 443 K exhibits wide range of linearity with the slope $a = 0.21$ which is close to exponent values reported in systems undergoing spinodal decomposition [18]. Values ranging from 1/6 to 1/3 were observed for crystalline metallic systems, while $a \approx 0.23$ was reported in a borate glass [18]. The slope of the plot for 463 K decreases rapidly finally reaching zero which is attributed to advanced crystallization blocking the decomposed regions coarsening.

The Cahn's linear theory of spinodal decomposition predicts an exponential growth of the SAXS intensity: $I(q) \propto |c - c_0|^2 \propto \exp(2R(q)t)$, where $c - c_0$ is the deviation from the homogeneous concentration c_0, $R(q)$ is the

q-dependent concentration fluctuation growth rate and t is time. The growth rate $R(q)$ is related to D – the modulus of the (negative) chemical interdiffusion coefficient ($D = |\tilde{D}|$) by: $R(q)/q^2 = D[1 - q^2/(2q_m^2)]$. Thus, by plotting $R(q)/q^2$ vs q^2 ("Cahn plot") one can obtain D from the straight line fit. While according to the linear theory of spinodal decomposition the "Cahn plot" should be a straight line, its' typically observed shape is not linear [18]. It was shown that the experimental data may be successfully analysed by looking at the tangents at the peak position q_m [22].

We have found that at T=443 K the SAXS intensity grows exponentially with time during inital 600 s. At higher temperatures the exponential fit was possible only for shorter times. Figure 5 shows the increase of the SAXS intensity at T=443 K for different values of q and the resulting "Cahn plot" is presented in Figure 6. Both from the tangent y axis itercept and the slope $D = 4 \cdot 10^{-21}$ [m^{2}s^{-1}] was obtained. The validity of this estimation can be checked by comparing the mean diffusion distance $\bar{x} = \sqrt{6Dt}$ with the characteristc dimension of the decomposed system. Using the evaluated value of D and t=7200 s, one gets $\bar{x} \approx 13$ nm which is in excellent agreement with the results from the Guinier method (see Figure 4).

Our previous results from X-ray diffraction and TEM [23] revealed that

$Al_{92}Sm_8$ glass devitrification kinetics is controlled by fcc-Al nanocrystal nucleation rate. The glass crystallization proceeds by gradual increase of crystallite density and decreasing average distance between crystals. At first, such a crystallization model appears to be inconsistent with present SAXS results. This apparent discrepancy can be resolved if one considers a coupling of amorphous phase separation and progressive crystallization of one of the decomposed phases. It can be reasoned that the SAXS interference maximum is partially due to spatially correlated amorphous regions and partially to nanocrystals nucleating preferentially inside the Al-rich zones. The local increase in the nucleation rate can be due to high Al diffusivity or/and reduced crystal-glass interfacial energy. The growth of the crystallites is constrained by the zone size because of the samarium atoms with sluggish atomic diffusion outside Al-rich regions. The decomposed structure coarsening proceeds parallel to crystallization which progressively further slows down glass decomposition. Our present results may reinforce some of the conclusions from electrical resistivity measurements [24] where considering of the amorphous phase decomposition gives better agreement with experimental data.

4 Conclusions

In conclusion, we suggest that amorphous phase separation is a mechanism triggering and controlling nanocrystallization of $Al_{92}Sm_8$ metallic glass. The model proposed here explains both high nucleation rate and rapid arrest of growth required for nanocrystalline microstructure formation.

5 Acknowledgments

J. Antonowicz gratefully acknowledges the Polish Committee of Scientific Research (grant no: 7T08 A02121) and Faculty of Physics of Warsaw University of Technology.

References

[1] C.-P.P. Chou, D. Turnbull, *J. Non-Cryst. Solids* **17** 169 (1975)

[2] S. Schneider, P. Thiyagarajan, W.L. Johnson, *Appl. Phys. Lett.* **68** 493 (1996)

[3] A.R. Yavari, *Acta. Metall.* **36** 1863 (1988)

[4] H.S. Chen, *Mater. Sci. Eng.* **23** 151 (1976)

[5] L. Tanner, R. Ray, *Scripta. Met.* **14** 657 (1980)

[6] R. Bush, S. Schneider, A. Peker, W.L. Johnson, *Appl. Phys. Lett.* **63** 1544 (1995)

[7] I. Martin, T. Ohkubo, M. Ohnuma, B. Deconihout, K. Hono, *Acta Mater.* **52** 4427 (2004)

[8] J. Löffler, W.L. Johnson, *Appl. Phys. Lett.* **76** 3394 (2000)

[9] U. Köster, *Mater. Sci. Forum* **235-238** 377 (1997)

[10] A. Inoue, *Progr. Mater. Sci.* **43** 365 (1998)

[11] M. Calin, U. Köster, *Mater. Sci. For.* **269-272** 749 (1998)

[12] G. Wilde, R.I. Wu, J.H. Perepezko, Proceedings of 22nd Risø International Symposium on Materials Science: Science of Metastable and Nanocrystalline Alloys Structure, Properties and Modelling, Editors: A.R. Dinesen, M. Eldrup, D. Juul Jensen, S. Linderoth, T.B. Pedersen, N.H. Pryds, A. Schrøoder Pedersen and J.A. Wert, Risø National Laboratory, Roskilde, Denmark 2001

[13] K.F. Kelton, *Phil. Mag. Lett.* **77** 337 (1998)

[14] T.K. Croat, A.K. Gangopadhyay, K.F. Kelton, *Phil. Mag. A* **82** 2483 (2002)

[15] K.F. Kelton, T.K. Croat, A.K. Gangopadhyay, L.-Q. Xing, A.L. Greer, M. Weyland, X. Li, K. Rajan, *J. Non-Cryst. Solids* **317** 71 (2003)

[16] T. Gloriant, D.H. Ping, K. Hono, A.L. Greer, M.D. Baró, *Mater. Sci. Eng.* **A304-306** 315 (2001)

[17] D.R. Allen, J.C. Foley, J.H. Perepezko, *Acta Mater.* **46** 431 (1998)

[18] K. Binder, P. Fratzl, *Spinodal Decomposition* in *Phase Transformations in Materials*, edited by G. Kostorz, pp. 409-480, Wiley-VCH, Weinheim, (2001).

[19] J. Antonowicz, *J. Non-Cryst. Solids* **351** 2383 (2005)

[20] A. Guinier and G. Fournet, *Small-Angle Scattering of X-Rays*, John Wiley & Sons, New York (1995)

[21] J.W. Cahn, *Acta Metall.* **9** 795 (1961)

[22] J.S. Langer, M. Bar-on, H.D. Miller, *Phys. Rev. A* **11** 1417 (1975)

[23] J. Antonowicz, A.R. Yavari, G. Vaughan, *Nanotechnology* **15** 1038 (2004)

[24] L. Łukaszuk, K. Pękała, *Nanotechnology* **16** 169 (2005)

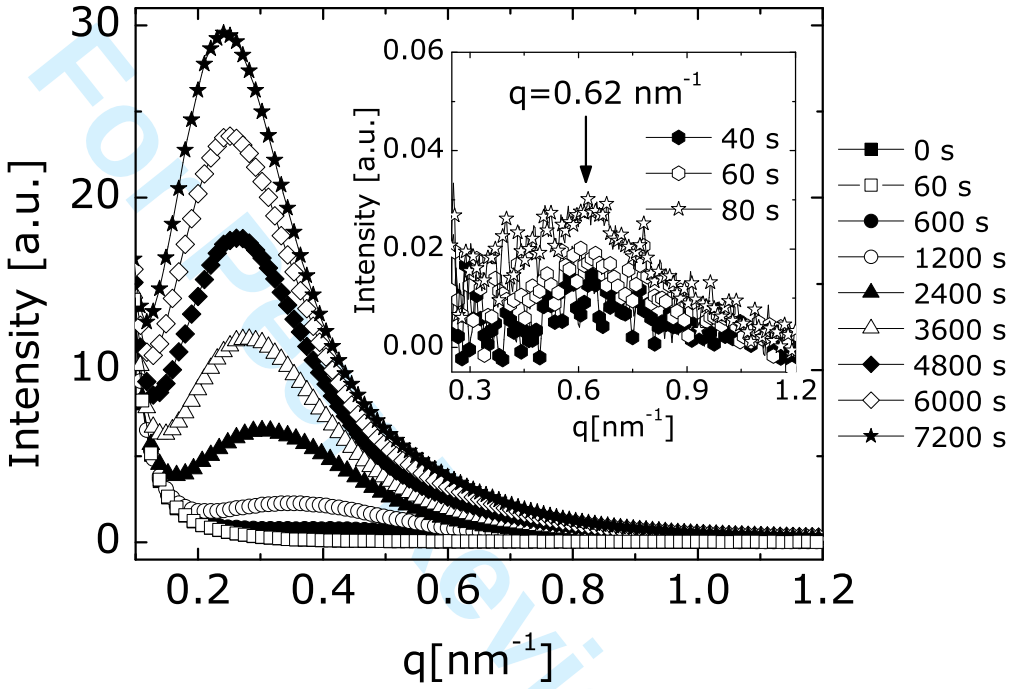

Figure 1: SAXS spectra evolution during isothermal annealing at 443 K of an as-quenched $Al_{92}Sm_8$. The inset presents early stages of SAXS maximum development when the peak is centered at $q = 0.62$ nm^{-1}.

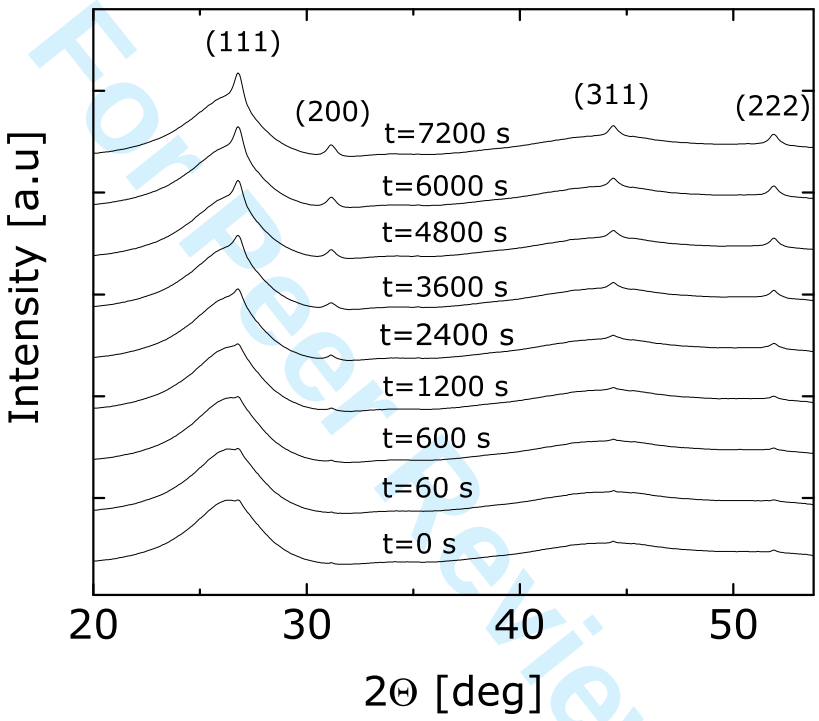

Figure 2: WAXS intensity data obtained during isothermal annealing at 443 K of an as-quenched $Al_{92}Sm_8$. The fcc-Al Bragg peaks are indexed.

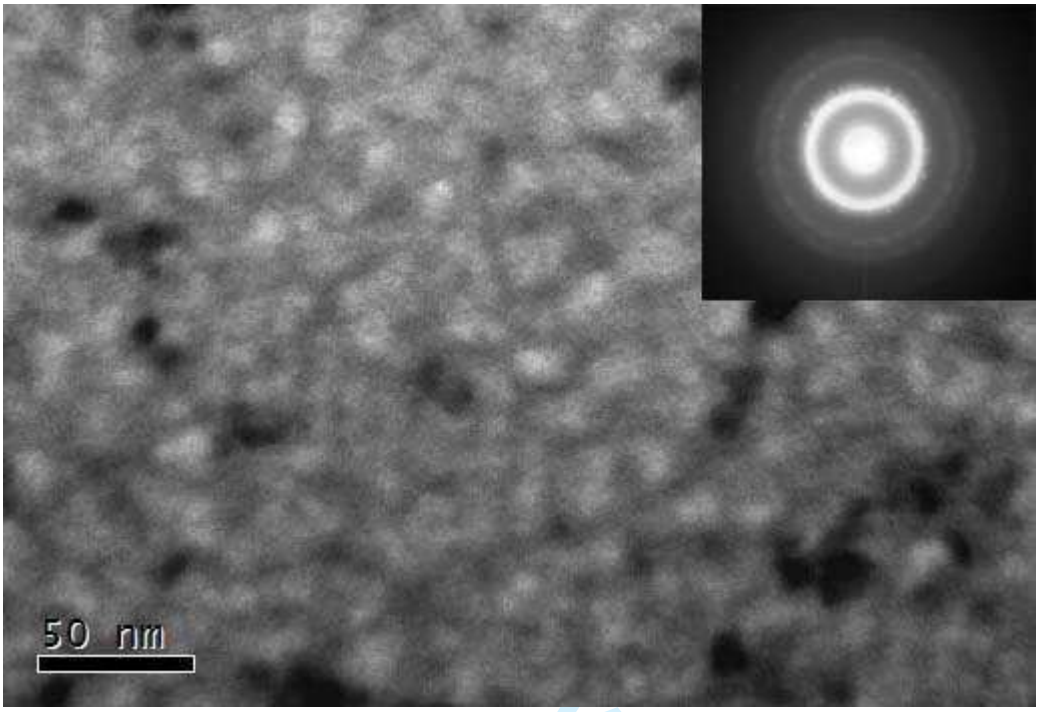

Figure 3: Bright field TEM image of $Al_{92}Sm_8$ glassy sample annealed at 460 K for 1200 s. The nanocrystal size determined from the micrograph is equal 11.5 ± 1.5 nm. The inset shows corresponding selected area diffraction pattern.

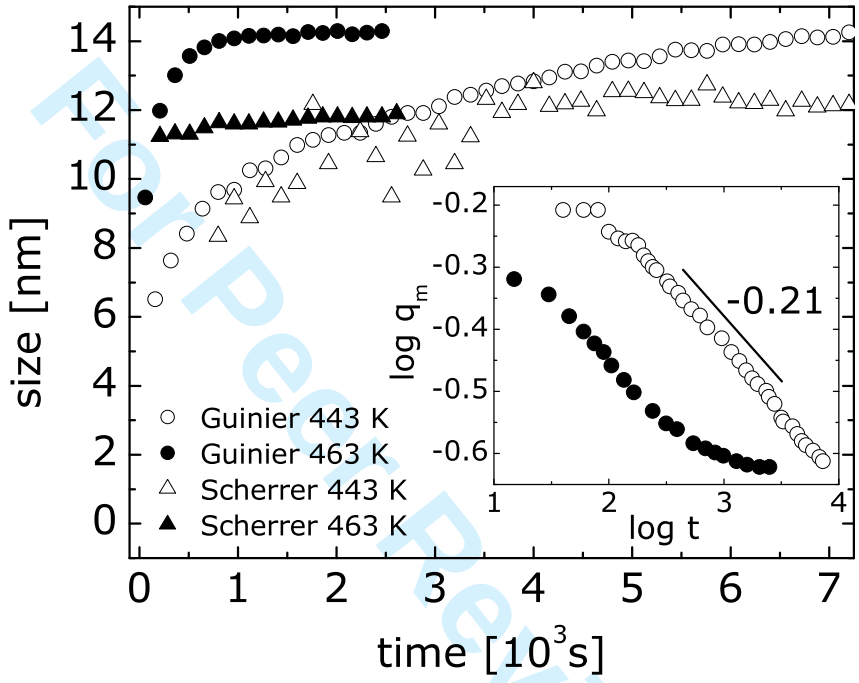

Figure 4: The compositional fluctuation size evolution obtained from the Guinier approximation (circles) and crystal size from the Scherrer method (triangles). The inset shows $\log q_m$ vs $\log t$ plot with the slope value indicated. Open symbols: annealing at 443 K, full symbols: annealing at 463 K.

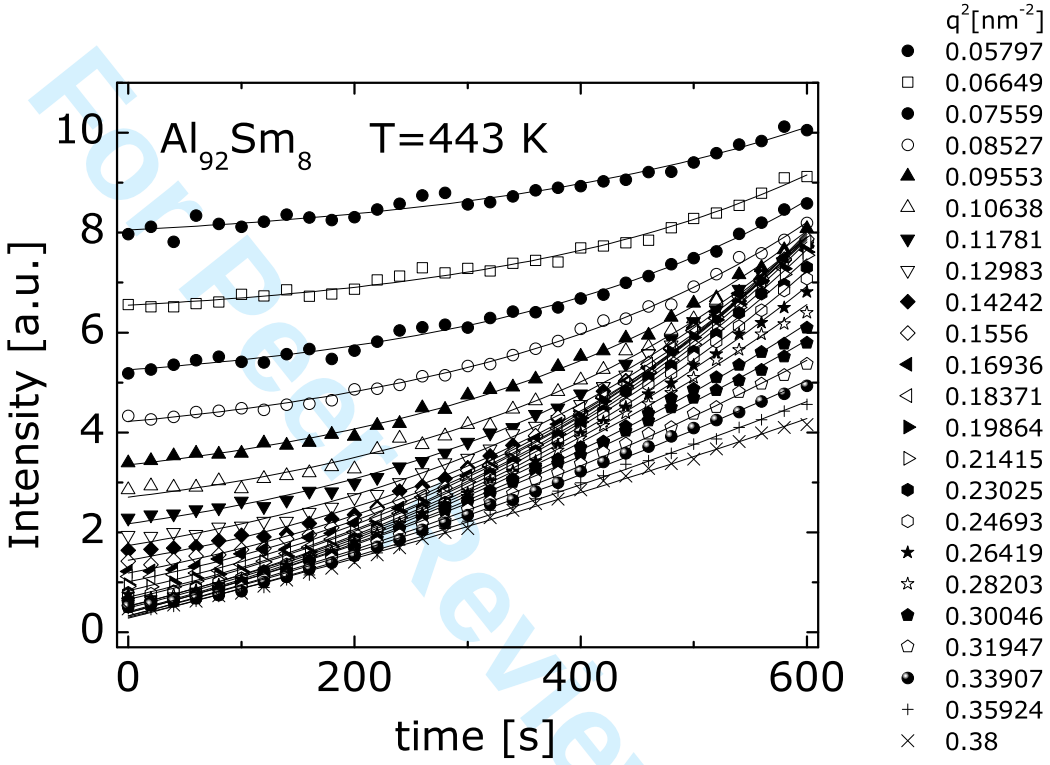

Figure 5: The increase of the SAXS intensity at T=443 K for different values of q (symbols). The lines are exponential fits.

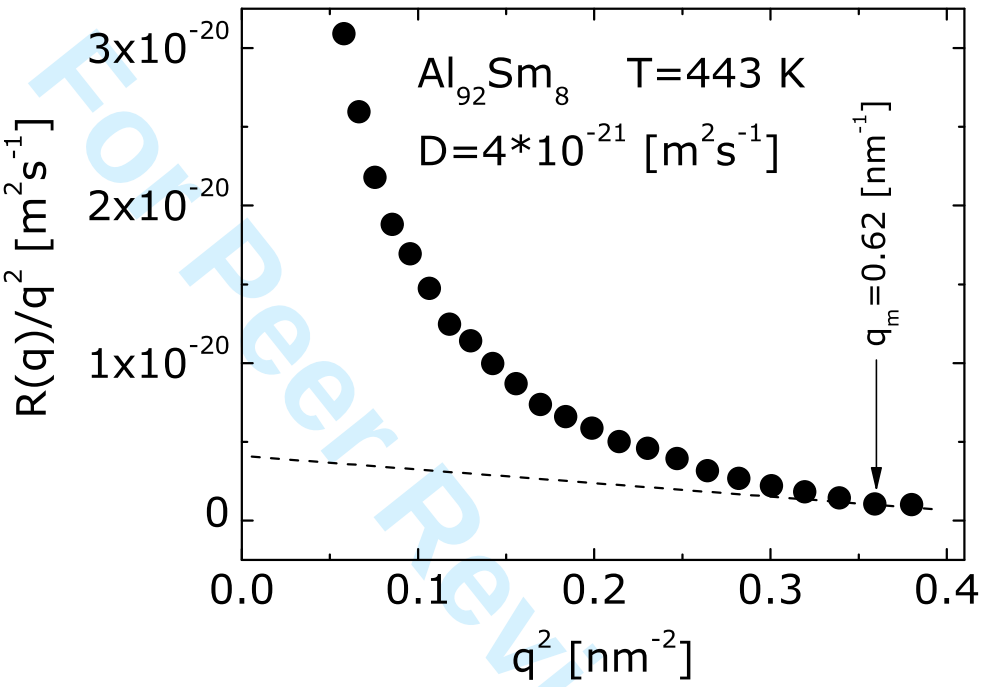

Figure 6: The "Cahn plot" obtained for T=443 K. The dashed line is a tangent to the curve at $q_m = 0.62$ nm $^{-1}$. The resulting diffusion coefficient is $D = 4 \cdot 10^{-21}$ [m^{2}s^{-1}]

List of Figures

6 The "Cahn plot" obtained for T=443 K. The dashed line is a tangent to the curve at $q_m = 0.62$ nm $^{-1}$. The resulting diffusion coefficient is $D = 4 \cdot 10^{-21}$ [m^{2}s^{-1}] 19